

# 1 Concurrent photochemical whitening and darkening of ambient 2 brown carbon

3 Qian Li<sup>1</sup>, Dantong Liu<sup>1\*</sup>, Xiaotong Jiang<sup>1</sup>, Ping Tian<sup>2</sup>, Yangzhou Wu<sup>1</sup>, Siyuan Li<sup>1</sup>, Kang Hu<sup>1</sup>, Quan Liu<sup>3</sup>,  
4 Mengyu Huang<sup>2</sup>, Ruijie Li<sup>2</sup>, Kai Bi<sup>2</sup>, Shaofei Kong<sup>4</sup>, Deping Ding<sup>2</sup>

5 <sup>1</sup>Department of Atmospheric Science, School of Earth Science, Zhejiang University, Hangzhou, 310027, China

6 <sup>2</sup>Beijing Key Laboratory of Cloud, Precipitation and Atmospheric Water Resources, Beijing Meteorological Service, Beijing,  
7 100089, China.

8 <sup>3</sup>State Key Laboratory of Severe Weather & Key Laboratory of Atmospheric Chemistry of CMA, Chinese Academy of  
9 Meteorological Sciences, Beijing, 100081, China

10 <sup>4</sup>Department of Atmospheric Science, School of Environmental Science, China University of Geosciences, Wuhan, 430074,  
11 China

12 *Correspondence to:* Dantong Liu (dantongliu@zju.edu.cn)

13 **Abstract.** The light-absorbing organic aerosol (OA), known as brown carbon (BrC), has important radiative impacts, however  
14 its sources and evolution after emission remain to be elucidated. In this study, the light absorption at multiple wavelengths,  
15 mass spectra of OA and microphysical properties of black carbon (BC) were characterized at a typical sub-urban environment  
16 in Beijing. The absorption of BC is constrained by its size distribution and mixing state and the BrC absorption is obtained by  
17 subtracting the BC absorption from the total aerosol absorption. Aerosol absorption was further apportioned to BC, primary  
18 BrC and secondary BrC by applying the least-correlation between secondary BrC and BC. The multi-linear regression analysis  
19 on the factorized OA mass spectra indicated the OA from traffic and biomass burning emission contributed to primary BrC.  
20 Importantly, the moderately oxygenated OA (O/C=0.62) was revealed to highly correlate with secondary BrC. These OA had  
21 higher nitrogen content, in line with the nitrogen-containing functional groups detected by the Fourier transform infrared  
22 spectrometer. The photochemical processes were found to result in reduced contribution of fraction of absorbance of primary  
23 BrC to total absorbance about 20% but enhanced contribution of secondary BrC by 30%, implying the concurrent whitening  
24 and darkening of BrC. This provides field evidence that the photochemically produced secondary nitrogen-containing OA can  
25 considerably compensate some bleaching effect on the primary BrC, hereby causing radiative impacts.

## 26 1. Introduction

27 Atmospheric absorbing organic aerosol (OA), known as brown carbon (BrC), is an important contributor to anthropogenic  
28 absorption besides black carbon (BC) (Laskin et al., 2015; Liu et al., 2020), particularly at shorter visible wavelengths (Bahadur  
29 et al., 2012). Due to complex compositions of OA, the primary sources and subsequent evolution of BrC in the atmosphere  
30 remains to be explicitly understood and causes uncertainties in evaluating the radiative impacts of BrC (Liu et al., 2020).

31 The chromophores of BrC are mainly aromatic compounds associated with certain functional groups (Liu et al., 2015c).  
32 Particularly, compounds containing nitro, nitrated or other forms of nitrogen-containing functional groups are more absorbing  
33 (Nakayama et al., 2013; Jacobson, 1999). It is well established that primary OA, especially from biomass burning, contains a  
34 large fraction of BrC (Andreae and Crutzen, 1997; Rizzo et al., 2013; Bond, 2001). These primary BrC has a range of  
35 absorptivity, which was found to be controlled by burning phases. OA co-emitting with BC (the flaming phase) exhibited a  
36 higher absorptivity than OA-dominated smoldering phase (Liu et al., 2021). BrC can experience reactions with atmospheric  
37 oxidants after emission. Previous studies (Satish et al., 2017; Satish and Rastogi, 2019; Dasari et al., 2019) found nitrogenous  
38 compounds from biomass burning were responsible for BrC over South Asia and the chromophores were photobleached in the  
39 afternoon. Numerous field and laboratory studies found the decrease of BrC absorptivity due to photobleaching of  
40 chromophores, with lifetime ranging from a few hours (Zhao et al., 2015; Liu et al., 2021) to a few days (Forrister et al., 2015),  
41 which may depend on the concentration of ambient hydroxyl radical (Wang et al., 2014), also influenced by relative humidity  
42 and particle volatility (Schnitzler et al., 2020). The absorptivity of BrC could be also enhanced due to addition of functional  
43 groups by forming conjugated structure with aromatics. This was supported by a number of laboratory studies that BrC  
44 absorptivity could be enhanced when forming nitrogen-containing organic compounds, such as the formation of nitro-  
45 aromatics when aromatics reacted with  $\text{NO}_x$  (Nakayama et al., 2013), or produced organic amine after reacting with ammonia  
46 (Updyke et al., 2012). The enhancement of BrC absorptivity could occur either through nitration of existing chromophores, or  
47 formation of new secondary organic aerosol (SOA) chromophores through gas-phase oxidation.

48 The above findings mean the enhancement or bleaching of BrC absorptivity via photooxidation will coexist. The time scale  
49 between both competing processes will ultimately determine the lifetime of BrC in the atmosphere. However, both processes  
50 have been rarely investigated in the field to explicitly determine the BrC components which principally determine the  
51 respective enhancement or decrease of its absorptivity, particularly in regions influenced by combined anthropogenic sources.  
52 In this study, by measurements using multiple-wavelength absorption and microphysical properties of BC in a sub-urban region,  
53 the absorption of BC, primary and secondary BrC was discriminated. In conjunction with source attribution via OA mass  
54 spectra, we are able to link the segregated absorption with certain sources and investigate their primary information and  
55 subsequent evolution. The competition between photobleaching and secondary formation of BrC was investigated in real world.

## 56 2. Experimental and instrumentation

## 57 2.1 Site description and meteorology

58 The experiment was conducted during springtime at the Beijing Cloud Laboratory and Observational Utilities Deployment  
59 Base (117.12°E, 40.14°N), which is located in the northeast suburban area in Beijing (Fig S1a). The site is surrounded by the  
60 northwest mountain ridge, without significant local primary anthropogenic emissions (Hu et al., 2021). The 72-h backward  
61 trajectories with every 3 hours initializing from the site are analyzed by the HYSPLIT model (Draxier and Hess, 1998) using  
62 the 3-hourly 1°×1° meteorological field from the GDAS reanalysis product. The obtained backward trajectories were further  
63 clustered to group the similar transport pathways (Makra et al., 2011). The meteorological parameters, including the  
64 temperature (T), ambient relative humidity (RH), wind speed (WS) and wind direction (WD) were measured by a monitoring  
65 station on the site.

## 66 2.2 Measurements of BC microphysics and absorption coefficient

67 In this study, the ambient aerosols were sampled by a large-flow (1.05 m<sup>3</sup> min<sup>-1</sup>) air particle sampler (TH-1000C II) with a  
68 PM<sub>2.5</sub> impactor (BGI SCC 1.829) and dried by a silica drier before measurement. The single particle soot photometer (SP2,  
69 DMT., USA) used continuous laser at  $\lambda=1064\text{nm}$  to incandescence light-absorbing aerosols (such as BC) for irradiating detectable  
70 visible light. The incandescence signal was used to measure the refractory black carbon (rBC) mass. The SP2 incandescence  
71 signal was calibrated using the Aquadag standard (Acheson Inc., USA), and a factor of 0.75 was applied to correct for ambient  
72 BC (Laborde et al., 2012). The scattering signal was calibrated by monodispersed polystyrene latex spheres (PSL). The BC  
73 core diameter ( $D_c$ ) was calculated from the measured BC mass by assuming a BC density of 1.8 g cm<sup>-3</sup> (Bond and Bergstrom,  
74 2006). The leading edge only (LEO) method was applied to reconstruct the scattering signal of BC, which was used to  
75 determine the coated particle diameter ( $D_p$ ) by a Mie-lookup table with the inputs of scattering and incandescence signal of  
76 each BC particle (Liu et al., 2014; Taylor et al., 2015). The mass median diameter (MMD) is derived from the  $D_c$  distribution,  
77 which is determined as below and above MMD the rBC mass concentration is equal (Liu et al., 2019a). The bulk coating  
78 thickness ( $D_p/D_c$ ) is calculated as the cubic root of ratio of the total coated BC volume divided by the total volume of rBC.

79 The mass absorption cross section (MAC) (in m<sup>2</sup> g<sup>-1</sup>) of each BC particle can be calculated using the measured coated and  
80 uncoated BC sizes by applying the Mie core-shell calculation. The absorption coefficient of BC at certain wavelength,  $\sigma_{\text{abs,BC}}$   
81 ( $\lambda$ ) is determined by multiplying the calculated MAC and rBC mass concentration at each size:

$$82 \sigma_{\text{abs,BC}}(\lambda) = \sum_i \text{MAC}(\lambda, D_{p,i}, D_{c,i}) m(\log D_{c,i}) \Delta \log D_{c,i} \quad (1)$$

83 where  $m(\log D_{c,i})$  denotes the BC mass concentration at each logarithmic bin of  $D_c$ . The SP2 measurement at  $\lambda=1064\text{nm}$  longer  
84 than mostly populated BC size means the derived coatings and subsequent calculation of MAC is relatively independent of  
85 particle shape within uncertainty of 21% (Liu et al., 2014; Hu et al., 2021).

86 The absorption coefficients at wavelengths  $\lambda= 375, 470, 528, 635$  and  $880$  nm were measured by a Micro-Aethalometer  
87 (MA200, Aethlabs, San Francisco, CA, USA). Aerosol particles were collected on filter tapes, on which the light attenuation  
88 was measured continuously with a time resolution of 30 s. The loading effect of filters was automatically corrected by

89 measuring attenuation at two different sampling flow rates on two spots in parallel (Drinovec et al., 2015a). Moreover, a multi-  
 90 scattering correction factor (C-value) of 3.5, 3.2 and 2.4 at the wavelengths 370 nm, 528 nm and 880 nm, respectively were  
 91 utilized to correct attenuation for the multiple light scattering effect. It was obtained by comparing the absorption coefficient  
 92 with a photoacoustic soot spectrometer (PASS-3, DMT) (Hu et al., 2021).

### 93 **2.3 Attribution of primary and secondary BrC absorption coefficient**

94 The absorption coefficient of BC at different  $\lambda$  is calculated using the measured uncoated core and coated size as mentioned  
 95 above. The absorption coefficient of total BrC is obtained by subtracting the BC absorption coefficient from the total absorption  
 96 at certain wavelength, expressed as:

$$97 \sigma_{\text{abs, BrC}}(\lambda) = \sigma_{\text{abs, total}}(\lambda) - \sigma_{\text{abs, BC}}(\lambda) \quad (2)$$

98 where the absorption coefficient of BC ( $\sigma_{\text{abs, BC}}$ ) is obtained from the SP2 measurement,  $\sigma_{\text{abs, total}}(\lambda)$  is the total light absorption  
 99 of aerosols measured by the MA200. The absorption coefficient of secondary BrC, the absorption not contributed by primary  
 100 sources, is obtained by subtracting the absorption of all primary sources from the total absorption (Crilley et al., 2015),  
 101 expressed as:

$$102 \sigma_{\text{abs, secBrC}}(\lambda) = \sigma_{\text{abs, total}}(\lambda) - \sigma_{\text{abs, pri}}(\lambda) \quad (3)$$

103 where  $\sigma_{\text{abs, pri}}(\lambda)$  is the light absorption from primary sources. Here an assumption is made that light absorption from primary  
 104 aerosols is all from combustion sources, and these sources necessarily contain BC (Wang et al., 2018a). Therefore, the total  
 105 absorption from primary sources can be obtained by scaling a factor from the mass concentration of BC, expressed as:

$$106 \sigma_{\text{abs, pri}}(\lambda) = \left( \frac{\sigma_{\text{abs, total}}}{[\text{rBC}]} \right)_{\text{pri}} \cdot [\text{rBC}] \quad (4)$$

107 where [rBC] is the mass concentration of rBC measured by the SP2,  $\left( \frac{\sigma_{\text{abs, total}}}{[\text{rBC}]} \right)_{\text{pri}}$  is the scaling factor to derive the  
 108 absorption of primary combustion sources from [rBC]. This factor is obtained using the minimum R-squared (MRS) approach  
 109 (Wu and Yu, 2016), by adjusting the factor until a minimum correlation between  $\sigma_{\text{abs, secBrC}}$  and [rBC] is reached because the  
 110 absorption from secondary sources are least likely to covary with that from primary sources (Wang et al., 2019a). This method  
 111 has been used in urban and sub-urban environment to obtain the primary BrC associated with combustion sources. Being  
 112 different from previous studies, an auxiliary characterization of rBC mass measured by the SP2 is used here to avoid the  
 113 possible interference from absorption measured by the same instrument. The  $\left( \frac{\sigma_{\text{abs, total}}}{[\text{rBC}]} \right)_{\text{pri}}$  ratio at  $\lambda=375$  nm, 470 nm, 528  
 114 nm, 635 nm and 880 nm is calculated to be 20.7, 17.0, 14.4, 11.7 and 5, respectively (Fig. S2), which falls within the reported  
 115 values from previous studies 11-50 (Zhang et al., 2020; Wang et al., 2019a). This scenario assumes a relatively consistent  
 116 absorption relative to BC mass concentration from sources during experiment. This however may not include some sporadic  
 117 events when sources with distinct OA or BC mass fraction may be introduced and alter the single  $\left( \frac{\sigma_{\text{abs, total}}}{[\text{rBC}]} \right)_{\text{pri}}$  ratio. The  
 118  $\sigma_{\text{abs, secBrC}}$  therefore represents the overall mean value during the experimental period but this ratio will vary with seasons and

119 locations. The  $\sigma_{\text{abs}}$  of primary BrC can then be calculated as:

$$120 \quad \sigma_{\text{abs,priBrC}}(\lambda) = \sigma_{\text{abs,BrC}}(\lambda) - \sigma_{\text{abs,secBrC}}(\lambda) \quad (5)$$

121 where  $\sigma_{\text{abs,BrC}}$  and  $\sigma_{\text{abs,secBrC}}$  is calculated from Equation (2) and (3), respectively.

## 122 **2.4 Composition measurement**

123 The mass concentration and chemical composition of non-refractory sub-micron PM (NR-PM<sub>1</sub>) including organic aerosols  
124 (OA), nitrate (NO<sub>3</sub><sup>-</sup>), sulfate (SO<sub>4</sub><sup>2-</sup>), chloride (Cl<sup>-</sup>) and ammonium (NH<sub>4</sub><sup>+</sup>) were determined with a High-Resolution Time-of-  
125 Flight Aerosol Mass Spectrometer (HR-ToF-AMS, Aerodyne Research Inc., USA). The setup, operation, and calibration  
126 procedures of the AMS have been described elsewhere (Canagaratna et al., 2007). During this field observation, the AMS was  
127 operated in V-mode for the quantification of mass concentrations. The composition-dependent collection efficiencies were  
128 applied ((Middlebrook et al., 2012), and the ionization efficiency was calibrated using 300 nm pure ammonium nitrate (Jayne  
129 et al., 2000). Elemental ratios of OA including oxygen-to-carbon (O/C), hydrogen-to-carbon (H/C) and nitrogen-to-carbon  
130 (N/C) were determined to the improved-ambient method (Canagaratna et al., 2015).

131 Positive Matrix Factorization (PMF) (Paatero and Tapper, 1994) was performed on the inorganic and organic high-resolution  
132 mass spectra to distinguish OA components from different sources (Zhang et al., 2011; Ulbrich et al., 2009; Decarlo et al.,  
133 2010). The mass spectra of the combined matrix for  $m/z < 120$  were excluded in PMF analysis. Five OA factors were identified.  
134 The diagnostics of PMF is summarized in Text S1 and Fig. S6.

## 135 **2.5 Offline Fourier transform infrared spectrometer (FTIR) analysis**

136 Particulate Matter (PM) samples were collected once a day onto prebaked (600°C, 4h) quartz fiber filters (Whatman, QMA,  
137 USA) using a large-flow (1.05 m<sup>3</sup> min<sup>-1</sup>) air particle sampler (TH-1000C II). The collected filter samples were stored in the  
138 refrigerator at -20°C before analysis. The infrared spectra of collected samples were measured by a Fourier transform infrared  
139 spectrometer (FTIR, Thermo Scientific, USA) equipped with an iD5 attenuated total reflectance accessory (diamond crystal)  
140 to quantify the chemical functional groups over the wavenumbers range of 550-4000 cm<sup>-1</sup> with a resolution of 0.5 cm<sup>-1</sup>. The  
141 NO and NO<sub>2</sub> symmetric stretch in the FTIR spectra can characterize the functional groups associated with nitrogen-containing  
142 organics (Coury and Dillner, 2008). Fig. S3 shows typical examples of FTIR spectra and the assigned functional groups for  
143 the three pollution levels during experiment. The peak at 1110 cm<sup>-1</sup> corresponds to the background of the quartz fiber filter  
144 overlapped with some X-H bending vibrations, which is subtracted for the following analysis. The characteristic organic nitrate  
145 spectra appear at wavenumbers 860 cm<sup>-1</sup> (NO symmetric stretch), 1280 cm<sup>-1</sup> (NO<sub>2</sub> symmetric stretch) and 1630-1640cm<sup>-1</sup>  
146 (NO<sub>2</sub> asymmetric stretch) (Bruns et al., 2010). After baseline calibration, The FTIR peaks of 1630cm<sup>-1</sup> and 860cm<sup>-1</sup> are  
147 integrated the absorption areas above the baseline. The summed integrated area of -NO and -NO<sub>2</sub> are hereby used to indicate  
148 the nitrogen-containing organics. There was no discernable peak of carbonyl group for our infrared spectrum, and the peak of  
149 OH at 2500 cm<sup>-1</sup> - 3400 cm<sup>-1</sup> for the carboxylic acid is not discernable neither, thus the influence of ketone and carboxylic acid

150 may be of less importance for our dataset.

### 151 3. Results and Discussion

#### 152 3.1 Source attributed OA

153 The overview results are shown in Fig. S1. The organics dominated the aerosol compositions for most time, but occasionally  
154 nitrate was the most abundant component (Fig. S1g). Note that the nitrate here may also include components containing in  
155 organics besides ammonium nitrate. Backward trajectories (Fig. S1a-d) showed that the most abundant PM<sub>1</sub> concentration was  
156 associated with air masses transported in shorter distance from southern regions (C1), but the longer and faster northerly  
157 transported air mass from cleaner north (C2) could dilute the concentrations.

158 The resolved OA factors by the PMF analysis are shown in Fig. 1, including the mass spectra, time series and diurnal profiles  
159 of each PMF factor with corresponded external and internal tracers. Three primary OA (POA) were identified as hydrocarbon-  
160 like OA (HOA), cooking-related OA (COA), biomass burning OA (BBOA), with O/C of 0.31, 0.18 and 0.39 respectively.  
161 These POA had considerable fraction of hydrocarbon fragments (C<sub>x</sub>H<sub>y</sub>), indicating their less aged status. The HOA profile was  
162 characterized by higher contributions of aliphatic hydrocarbons and has dominated ion tracers such as *m/z* 41 (C<sub>3</sub>H<sub>5</sub><sup>+</sup>), 43  
163 (C<sub>3</sub>H<sub>7</sub><sup>+</sup>), 55 (C<sub>4</sub>H<sub>7</sub><sup>+</sup>) and 57 (C<sub>4</sub>H<sub>9</sub><sup>+</sup>). The HOA concentration correlated with BC (*r*=0.62), which emits from traffic emissions.  
164 The diurnal variation exhibited strong morning and afternoon rush-hour peaks of mass concentration. This factor was consistent  
165 with the mass spectra of previously measured HOA from on-road vehicle emissions in urban cities (Zhang et al., 2005; Aiken  
166 et al., 2009; Sun et al., 2016; Hu et al., 2017), which has *m/z* peaks characteristic of hydrocarbon fragments in series of C<sub>n</sub>H<sub>2n+1</sub><sup>+</sup>  
167 and C<sub>n</sub>H<sub>2n-1</sub><sup>+</sup>. The mass spectrum of HOA shows overall similarity to those of primary OA emitted from gasoline and diesel  
168 combustion sources (*r*=0.68) (Elser et al., 2016).

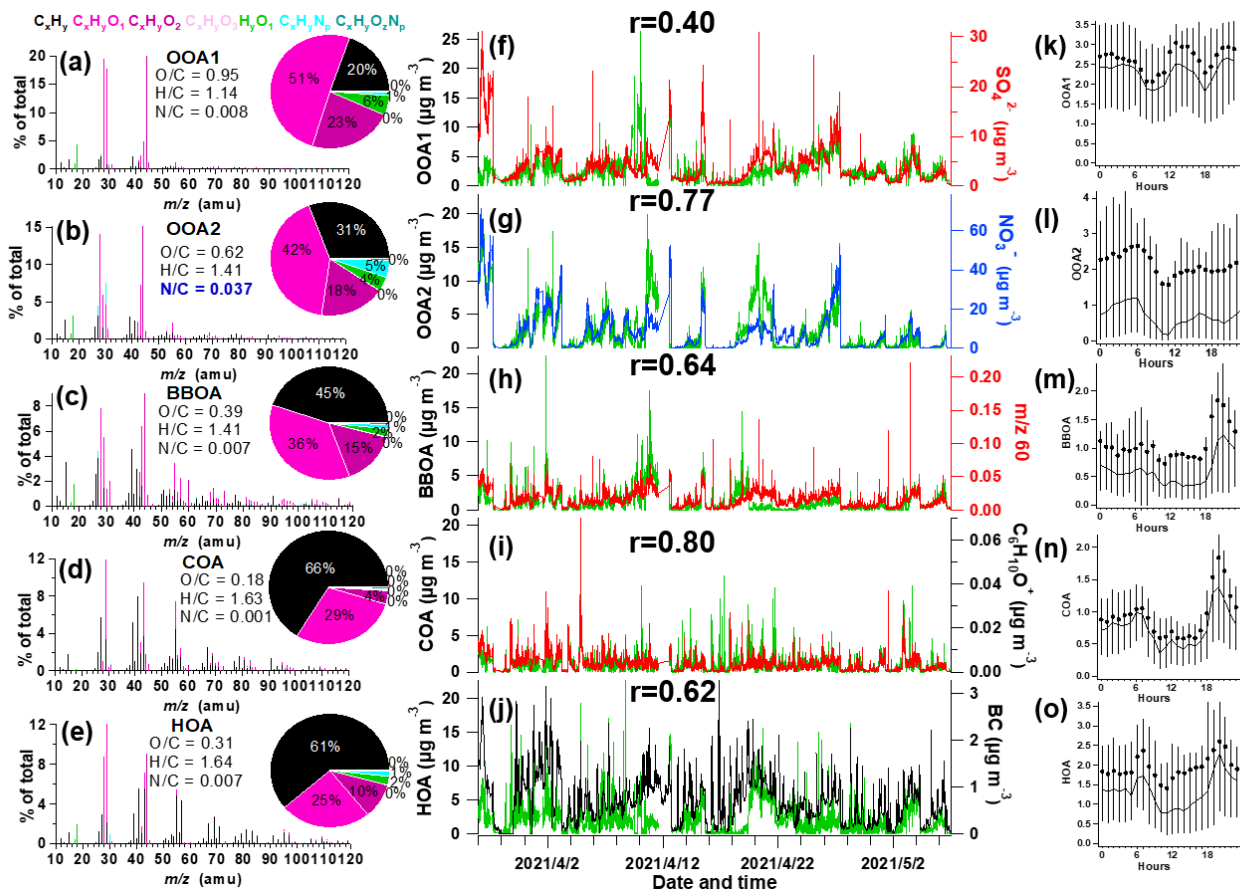
169 The OA from cooking sources (COA) is also characterized by prominent hydrocarbon ion series, however, with higher signal  
170 at C<sub>n</sub>H<sub>2n-1</sub><sup>+</sup> than C<sub>n</sub>H<sub>2n+1</sub><sup>+</sup>. COA had apparent fragments of both C<sub>4</sub>H<sub>9</sub><sup>+</sup> and C<sub>3</sub>H<sub>3</sub>O<sup>+</sup>, and has a higher ratio of C<sub>3</sub>H<sub>3</sub>O<sup>+</sup>/C<sub>3</sub>H<sub>5</sub>O<sup>+</sup>  
171 (3.1), C<sub>4</sub>H<sub>7</sub><sup>+</sup>/C<sub>4</sub>H<sub>9</sub><sup>+</sup> (2.2) than HOA (0.9–1.1), with cooking-related fragments of C<sub>5</sub>H<sub>8</sub>O<sup>+</sup> (*m/z* 84), C<sub>6</sub>H<sub>10</sub>O<sup>+</sup> (*m/z* 98) and  
172 C<sub>7</sub>H<sub>12</sub>O<sup>+</sup> (*m/z* 112) (Sun et al., 2011b; Mohr et al., 2012). The COA shows overall similar spectral pattern to the reference  
173 spectra of COA (*r*=0.92) (Elser et al., 2016). Its minor peak at noon and larger peak in the evening (Fig. 11) also corresponded  
174 with the lunch and dinner time respectively. There was only a minor peak at noon for COA, which may be due to the sub-urban  
175 nature of the site where the major aerosols from cooking sources may have been processed and lost the signature near source.  
176 The feature of this factor was also observed in sub-urban environment (Huang et al., 2021).

177 The BBOA factor was identified based on the prominent signals of *m/z* 60 (C<sub>2</sub>H<sub>4</sub>O<sub>2</sub><sup>+</sup>) and 73(C<sub>3</sub>H<sub>5</sub>O<sub>2</sub><sup>+</sup>), which are known  
178 fragments of levoglucosan (Cubison et al., 2011). And BBOA also correlated with potassium (K<sup>+</sup>, *r* = 0.80), which are indicator  
179 of biomass burning (Pachon et al., 2013; Brown et al., 2016). The *m/z* 60 and 73 together with a unique diurnal variation have  
180 been shown to be a robust marker for the presence of aerosols from biomass burning emissions in many urban locations (Sun

181 et al., 2016). The BBOA shows very similar mass spectral patterns to previously reported reference spectra of biomass burning  
182 ( $r=0.94$ ) (Elser et al., 2016). The BBOA factor that was identified in spring accounted for 12.8% of the total OA in Beijing,  
183 similar to previous reports (Hu et al., 2017). Biomass (Cheng et al., 2013) and solid fuel burning emissions (Sun et al., 2014)  
184 have been widely observed to importantly contribute to the primary OA in this region. This off-road combustion source was  
185 particularly abundant during wintertime for residential heating activities (Shen et al., 2019; Yang et al., 2018; Liu et al., 2016),  
186 while boiler for industry use (mostly using coal as fuel) was in operation throughout the year (Liu et al., 2015b). During the  
187 springtime of the experiment, the residential heating activities dropped due to increased ambient temperature thus the BBOA  
188 may be mainly contributed by the industry sector.

189 Two types of oxygenated organic aerosols (OOA) were identified, in moderate (OOA2,  $O/C=0.62$ ) and high oxidation state  
190 (OOA1,  $O/C=0.95$ ), respectively, which is very similar to the spectra of OOA factors resolved in other cities (Hayes et al.,  
191 2013; Ulbrich et al., 2009). The average mass spectrum of OOA2 in this study is characterized by  $m/z$  29 (mainly  $\text{CHO}^+$ ), 43  
192 (mainly  $\text{C}_2\text{H}_3\text{O}^+$ ) and  $m/z$  44 ( $\text{CO}_2^+$ ), similar to the semi-volatile OOA spectrum identified in other locations (Sun et al., 2011a;  
193 Zhou et al., 2016). On average, OOA2 accounts for 42% and 18% of  $\text{C}_x\text{H}_y\text{O}^+$  and  $\text{C}_x\text{H}_y\text{O}_2^+$  ions, respectively (Fig. 1b). These  
194 results clearly indicate that OOA2 was primarily composed of less oxygenated, possibly freshly oxidized organics. Notably,  
195 OOA2 had a substantially higher  $N/C$  than other factors ( $N/C=0.037$ ), and had highest correlation with nitrate ( $r=0.77$ ) and  
196 with  $\text{C}_x\text{H}_y\text{N}_z$  and  $\text{C}_x\text{H}_y\text{N}_z\text{O}_p$  fragments ( $r=0.83$ ). This factor therefore tends to largely result from nitrogen-containing OA and  
197 its elevation at night may be also associated with dark oxidation by nitrate radical.

198 The mass spectrum of OOA1, which was characterized by a dominant peak at  $m/z$  44 (mainly  $\text{CO}_2^+$ ), a highest  $O/C$  (0.95). On  
199 average, OOA1 contributes 51% of the  $\text{C}_x\text{H}_y\text{O}^+$  signal and 23% of the  $\text{C}_x\text{H}_y\text{O}_2^+$  signal (Fig. 1a). OOA1 showed particularly  
200 high correlation with sulfate ( $r=0.40$ ) because of their similar volatilities (Huffman et al., 2009; Jimenez et al., 2009). The  
201 slight enhancement at noon for OOA1 (also for OOA2) soon after morning rush-hour indicated the likely rapid formation of  
202 SOA through photooxidation. This significantly higher mean OOA2 than median value in the diurnal pattern indicated that  
203 this OA type was largely associated with pollution events. Both OOA1 and OOA2 showed nighttime peak maybe due to  
204 reduced boundary layer.



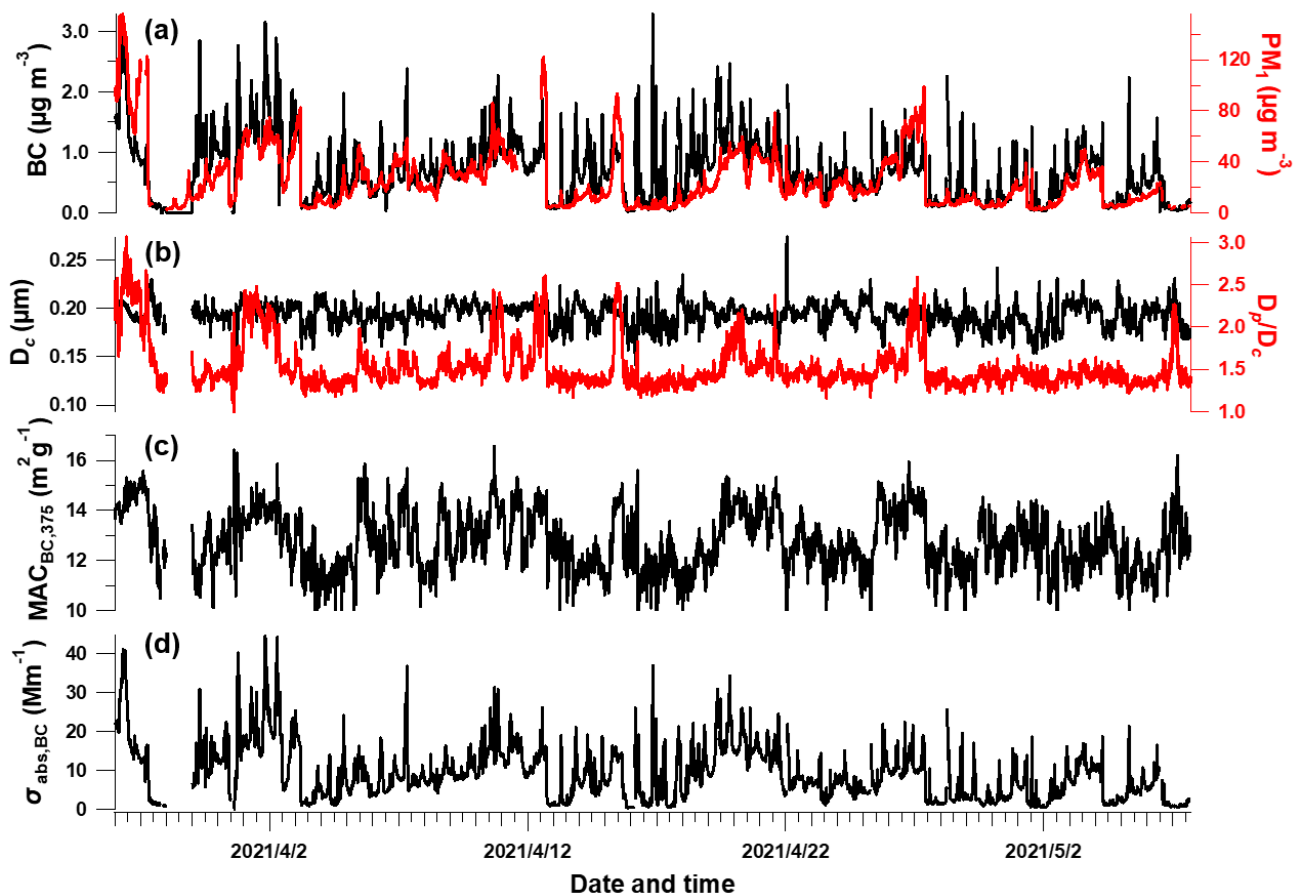
205  
206 **Figure 1. Information of source-apportioned organic aerosols by the PMF analysis. Mass spectra of (a) oxygenated OA1 (OOA1), (b)**  
207 **oxygenated OA2 (OOA2), (c) biomass burning OA (BBOA), (d) cooking-related OA (COA), (e). hydrocarbon-like OA (HOA), (f-j)**  
208 **Temporal variations of each PMF factor and the corresponding marker species. (k-o) Diurnal profiles of each factor. The lines, dots**  
209 **and whiskers denote the median, mean and the 25th/75th percentiles at each hour respectively.**

### 210 3.2 Segregated aerosol absorption

211 Fig. 2 shows the time series of BC properties, including the BC mass concentration,  $D_p/D_c$ ,  $D_c$ , MAC and light absorption  
212 coefficient of BC (section 2.2). The MMD of BC core varied between 93 – 274 nm which may correspond to the source-  
213 specific information (Liu et al., 2019b) or coagulation process during ageing. The coating of BC (indicated by  $D_p/D_c$ ) showed  
214 sporadic enhancement which was closely associated with enhanced PM concentration (Fig. 2a). This was consistent with  
215 previous studies that high coatings of BC occurred during heavier pollution due to the enhanced secondary formation of  
216 condensable materials to particle phase (Ding et al., 2019; Zhang et al., 2018). This clearly indicates the variation of mixing  
217 state of BC and this will potentially influence its MAC and absorption Ångström exponent (AAE) (Liu et al., 2015a). It will  
218 introduce considerable uncertainties to use constant MAC or AAE to derive the absorption coefficient of BC at multiple  
219 wavelengths. The MAC estimated using the measured BC core size and coatings (Fig. 2c) is thus used to derive the  $\sigma_{\text{abs,BC}}$   
220 (section 2.2, shown in Fig. 2d). The  $\sigma_{\text{abs,BC}}$  was  $9.1 \pm 7.3 \text{ Mm}^{-1}$  during experimental period. MAC of BC at  $\lambda=375\text{nm}$  showed to



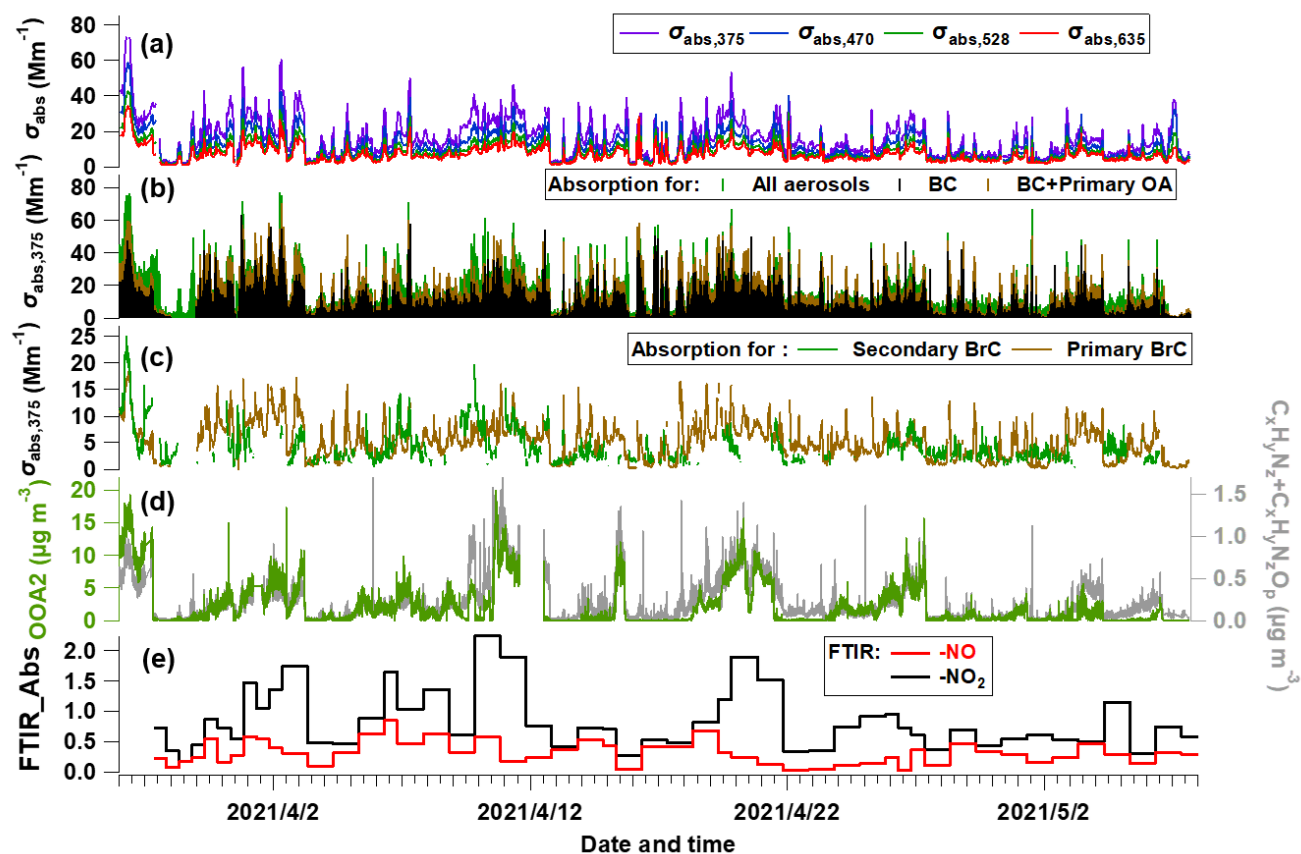
221 be at  $8.4 - 16.6 \text{ m}^2 \text{ g}^{-1}$  with enhanced absorption when high coatings, which was consistent with previous studies which reported  
 222  $\text{MAC}_{\text{BC}}$  of  $8-10 \text{ m}^2 \text{ g}^{-1}$ , and higher value of  $9.7 - 17.2 \text{ m}^2 \text{ g}^{-1}$  under polluted condition (Ding et al., 2019; Hu et al., 2021). The  
 223 uncertainty of  $\left(\frac{\sigma_{\text{abs,total}}}{[\text{rBC}]_{\text{pri}}}\right)$  is 4% for the data points over 1.5 according to (Wang et al., 2019a). The measurement of rBC  
 224 mass from the SP2 had uncertainty of 20% (Schwarz et al., 2008), with relative coating thickness having uncertainty of 23%  
 225 (Taylor et al., 2015), hereby resulting in a uncertainty of 27% for calculated  $\text{MAC}_{\text{BC}}$ . The above results in uncertainties of 31%  
 226 and 20% for  $\sigma_{\text{abs,BC}}$  and  $\sigma_{\text{abs,pri}}$ , respectively. The absorption measurement by MA200 had uncertainty of 25% (Drinovec et al.,  
 227 2015b; Duesing et al., 2019). All these uncertainties propagates the uncertainties of  $\sigma_{\text{abs,BrC}}$ ,  $\sigma_{\text{abs,priBrC}}$  and  $\sigma_{\text{abs,secBrC}}$  as 40%, 37%  
 228 and 32% respectively. These are summarized in Table S1.



229 **Figure 2. Temporal evolution of BC-related properties. (a) rBC and  $\text{PM}_{10}$  mass concentration, (b) BC core diameter and bulk coating**  
 230 **thickness ( $D_p/D_c$ ), (c) calculated mass absorption cross section (MAC) at  $\lambda=375\text{nm}$ , (d) absorption coefficient of BC.**  
 231

232 Using the method above, the total ( $\sigma_{\text{abs,total}}$ ) and attributed absorption of BC ( $\sigma_{\text{abs,BC}}$ ), primary ( $\sigma_{\text{abs,priBrC}}$ ) and secondary BrC  
 233 ( $\sigma_{\text{abs,secBrC}}$ ) at  $\lambda=375\text{nm}$  are shown in Fig. 3a-c. In Fig. 3b, the brown and green shades above the adjacent tracer indicate the  
 234 absorption coefficient of primary and secondary BrC, respectively. Fig. 3c shows that the absorption coefficient of primary

235 BrC was higher than secondary BrC for most time, but for certain periods they were equivalent or secondary BrC occasionally  
 236 exceeds primary BrC. The mean contribution of absorption coefficient for BC, primary BrC and secondary BrC is 51%, 27%  
 237 and 22% in this study. The tracers associated with nitrogen-containing organics, such as OOA2 (with highest N/C),  $C_xH_yN_z$   
 238 and  $C_xH_yN_zO_p$  fragments, and the FTIR measured  $-NO + -NO_2$ , are also shown in Fig. 3d-e.



239  
 240 **Figure 3. Temporal evolution of segregated absorbing properties.** (a) Absorbing coefficients ( $\sigma_{abs}$ ) at multiple wavelengths measured  
 241 by the aethalometer, (b)  $\sigma_{abs}$  at  $\lambda=375nm$  ( $\sigma_{abs,375}$ ) for all aerosols, primary OA and BC, (c)  $\sigma_{abs,375}$  for primary BrC and secondary  
 242 BrC. (d) mass concentration of OOA2 and the  $C_xH_yN_z$  and  $C_xH_yN_zO_p$  fragments measured by the AMS. (e) FTIR-measured  
 243 absorption of  $-NO$  and  $-NO_2$  bonds.

### 244 3.3 Source attribution of BrC absorption

245 A multiple linear regression (MLR) analysis is performed to apportion the absorption coefficient of BrC with the PMF  
 246 attributed OA factors, expressed as:

$$247 \sigma_{abs,BrC} = a_0 + a_1 \cdot [OOA1] + a_2 \cdot [OOA2] + a_3 \cdot [BBOA] + a_4 \cdot [COA] + a_5 \cdot [HOA] \quad (6)$$

248 where  $a_1$  to  $a_5$  represents the regression coefficients for each factor. The contribution of each source-specific OA factor to  
 249  $\sigma_{abs,BrC}$  can be obtained. This analysis is performed for the total BrC, primary and secondary BrC respectively. The results are  
 250 shown in Table 1. MLR on the total BrC shows relatively higher correction ( $r > 0.4$ ) with the factors of HOA, BBOA and OOA2,

251 suggesting the potential importance of the primary biomass burning and traffic source along with OOA2 in governing  
 252 absorption of BrC. MLR analysis on the primary BrC distinguishes its substantial correlation with BBOA ( $r=0.40$ ) and HOA  
 253 ( $r=0.46$ ), while MLR on the secondary BrC has a high correlation with OOA2 only ( $r=0.44$ ). The MLR analysis links the  
 254 apportioned absorption of physical properties with source-attributed chemical compositions, therefore validating and  
 255 identifying the sources of primary and secondary BrC.

256 **Table 1. Results of the multilinear regression analysis (MLR) between  $\sigma_{\text{abs},375}$  and the five PMF-resolved OA factors, with  $\sigma_{\text{abs},375}$  of**  
 257 **total BrC, primary and secondary BrC as dependent, respectively. All regression coefficients have passed the significance test with**  
 258  **$p<0.01$ . Partial correlations above 0.4 are marked in bold. Since negative values appear when the COA participates, which is thus**  
 259 **not included in the final regression but the values using COA factor are shown in brackets.**

Dependent	$\sigma_{\text{abs,BrC}}$		$\sigma_{\text{abs,pri BrC}}$		$\sigma_{\text{abs,sec BrC}}$	
Model	Regression coefficient	Partial correlation	Regression coefficient	Partial correlation	Regression coefficient	Partial correlation
Constant	2.26		1.67		1.47 (1.52)	
OOA1	0.57	0.23	0.04	0.02	0.46(0.46)	0.24 (0.24)
OOA2	1.22	<b>0.53</b>	0.37	0.25	0.74 (0.74)	<b>0.44 (0.44)</b>
BBOA	2.59	<b>0.46</b>	1.22	<b>0.40</b>	1.14 (1.18)	0.29 (0.29)
COA	1.30	0.22	1.45	0.36	/ (-0.25)	/ (-0.05)
HOA	1.70	<b>0.47</b>	1.17	<b>0.46</b>	0.49 (0.52)	0.20 (0.21)
R <sup>2</sup>	0.77		0.63		0.55 (0.55)	

260 Importantly, an oxygenated secondary OA factor (OOA2) is identified to significantly contribute to the secondary BrC. This  
 261 OOA has a moderate O/C (0.62) and a highest N/C of 0.037 among all factors. The high N/C means this factor contains the  
 262 most abundant nitrogen-containing fragments, implied as its high correlation with the  $\text{C}_x\text{H}_y\text{N}_z$  and  $\text{C}_x\text{H}_y\text{N}_z\text{O}_p$  fragments ( $r=0.83$ ,  
 263 Fig. 3d) and with the FTIR absorption for -NO<sub>2</sub> and -NO bonds ( $r=0.69$ , Fig. S4). The -NO bond is mostly related to the  
 264 organic nitrates (RONO<sub>2</sub>), and -NO<sub>2</sub> peak could result from both organic nitrates and nitro-organics (Bruns et al., 2010). There  
 265 is no discernable peak for organic amines. These all consistently imply that the OOA2 factor contained substantial fraction of  
 266 nitrogen-containing organics, and these compounds have contributed to the absorption of secondary BrC.

### 267 3.4 Simultaneous whitening and darkening process of BrC

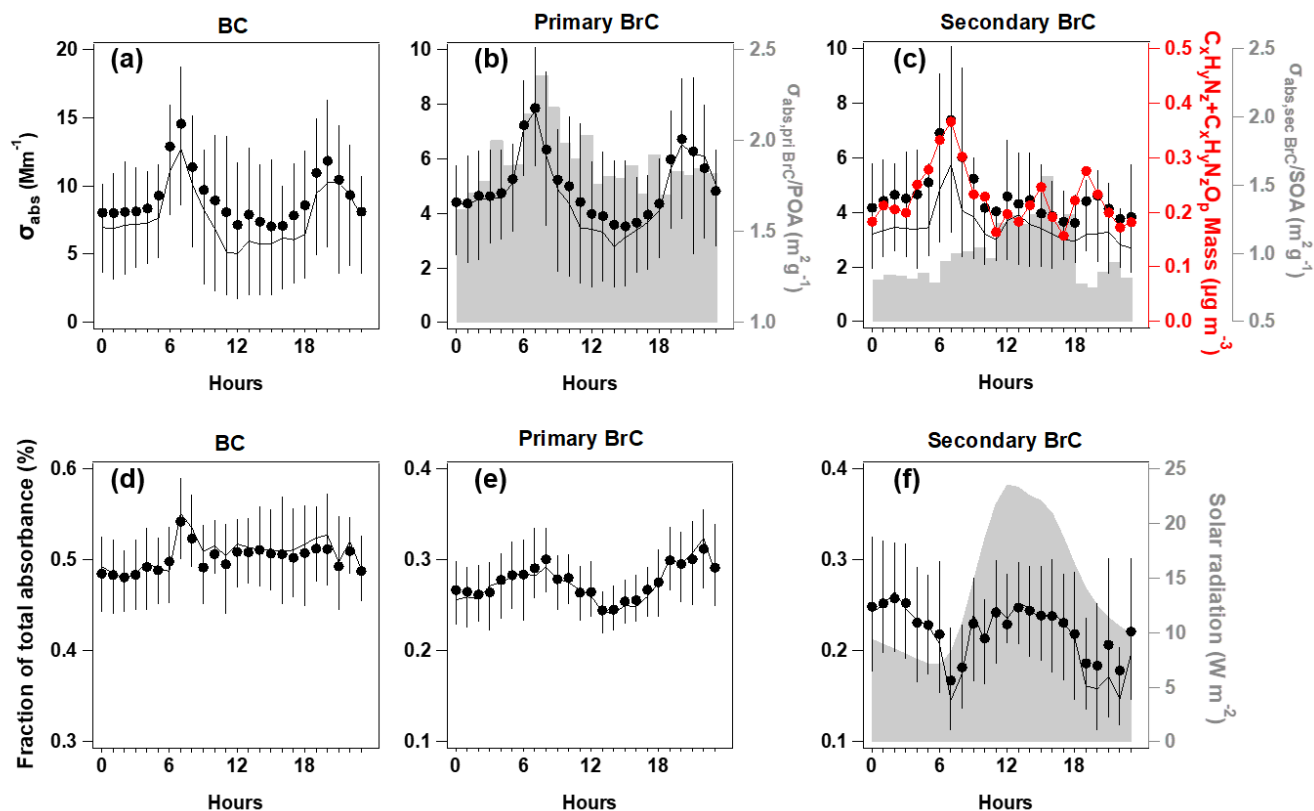
268 The relative contribution and diurnal variation of primary and secondary BrC measured by MA200 at 470, 528 and 635nm  
 269 wavelengths are similar to those at 375nm wavelengths, but with decreased fraction of BrC absorption with increased  
 270 wavelength. The mean AAE of total BrC, primary BrC and secondary BrC is obtained by power fitting on the mean absorption  
 271 coefficient during the experiment (Fig.S7), which is 6.16, 5.69 and 6.40 respectively. This is consistent with other studies that

272 SOA usually had a higher AAE than POA (Gilardoni et al., 2016; Jiang et al., 2022). Due to the high contribution of BC to total  
273 absorption (>50% even at shortest wavelength), the spectral dependence of absorption in bulk has not shown apparent diurnal  
274 variation. The diurnal variation of  $\sigma_{\text{abs},375}$  for BC and primary BrC and their fractions showed consistent morning rush-hour  
275 peaks at 6:00-8:00 and the night-time enhancement due to reduced boundary layer (Fig. 4a-b). This was in line with the morning  
276 peak of HOA and night peak of BBOA. The traffic source in this region, in particular the diesel vehicles, was reported to emit  
277 considerable OA with certain chromophores, such as aromatics (Yao et al., 2015) and heterocyclic organic compounds (Gentner  
278 et al., 2017; Schuetzle, 1983). In the morning rush-hour, BC and primary BrC accounted for  $51\pm4\%$  and  $29\pm4\%$  in the total  
279  $\sigma_{\text{abs},375}$  respectively, with the remaining  $20\pm2\%$  classified as secondary BrC. The morning peak coinciding with the primary  
280 BrC may result from the rapid formation of BrC from sources when emitted gases condensed and formed aerosols. These may  
281 lead to high cooccurrence between primary and secondary BrC. Previous studies in urban environment also observed  
282 concurrent peaks of primary and secondary BrC, which usually occurred at morning rush hour (Zhang et al., 2020).  
283 Furthermore, the assumption of the method used to apportion primary and secondary BrC will cause some error in the  
284 distinction of absorption coefficient, it is possible that some of the primary sources are being attributed to secondary sources  
285 and vice versa. This maybe a possible reason for the simultaneous peak observed for primary and secondary BrC during  
286 morning rush hour. The night had contributions from BC and primary BrC at  $50\pm2\%$  and  $30\pm3\%$  respectively, with  $20\pm3\%$  as  
287 secondary BrC. Fig. 4b showed the decrease of primary BrC absorption tended to be more rapid than the HOA and BBOA  
288 mass (even a slight increase for HOA Fig. 1m and Fig. 1o) in the midday, leading to decreased absorption coefficient per unit  
289 mass of primary BrC (shade in Fig. 4b), which indicates the decrease of BrC absorptivity likely due to photochemistry. This  
290 may involve the OH radical reaction with existing chromophores in aerosol phase (Schnitzler et al., 2020) or by enhanced  
291 evaporation of aerosols to gas phase (Palm et al., 2020) leading to further decrease of BrC absorptivity during midday. In  
292 addition to photobleaching, it possible that some primary species transformed into less absorbing secondary BrC species.  
293 During this period, the type of HOA or BBOA that contribute to absorption may also have a lower absorptivity. In this context,  
294 a recent chamber study reported that the primary BrC from biomass burning plumes could be bleached to half of the initial  
295 absorptivity in 2-3 hours (Liu et al., 2021). The reaction of BrC with OH radical has been widely recognized as the main  
296 pathway for the loss of primary BrC absorptivity (Liu et al., 2020), and was parameterized as an exponential decrease with  
297 time at certain OH radical concentration in global scale (Wang et al., 2018b).

298 Besides the morning rush-hour peak, there was an early afternoon peak for the absorption coefficient of secondary BrC,  
299 prevailing the dilution effect of daytime boundary layer (Fig. 4c-S5). The night and morning peak of OOA2 and the morning  
300 peak of  $\sigma_{\text{abs,secBrC}}$  may result from primarily emitted moderately oxygenated OA, which was reported from some diesel sources  
301 (Dewitt et al., 2015; Gentner et al., 2012). The fraction of secondary BrC thus had a pronounced early afternoon peak soon  
302 after the peak solar radiation (Fig. 4f) and a peak after midnight soon after the nighttime peak of primary BrC (Fig. 4e). Fig  
303 4e-f shows the photochemical processes led to an enhanced contribution of secondary BrC to the total absorption by 30% from  
304 the morning rush-hour to midday, but during the same time reduced the contribution of primary BrC to the total absorption  
305 about 20%. This shift of peaking time from primary to secondary BrC demonstrates the likely process of SOA formation from

306 gases, and these SOA compounds containing nitrogen (i.e., the OOA2) considerably contributed to the light absorption. This  
307 ageing or oxidation likely occurred through photooxidation during early afternoon and aqueous processes (high RH conditions  
308 prevail during nighttime) during nighttime. The oxidized volatile organic compounds (VOCs) with nitrogen chemistry involved  
309 could condense to produce additional mass in particle phase (Ehn et al., 2014; Finewax et al., 2018). Due to the high NO<sub>x</sub>  
310 emission, photooxidation of traffic VOCs may have largely involved nitrogen chemistry. Previous studies found the NO<sub>x</sub>-  
311 involved SOA could produce considerable chromophores (Lin et al., 2015; Siemens et al., 2022), such as the traffic VOCs may  
312 produce SOA in a time scale of hours, containing nitro-aromatics (Wang et al., 2019b; Keyte et al., 2016). The daytime  
313 formation of organic nitrate may follow the gas-phase photooxidation mechanism, in which the excess NO could add to the  
314 peroxy radical to produce organic nitrate (Liebmann et al., 2019). The nighttime chemistry involving NO<sub>3</sub> radical through the  
315 oxidation of NO<sub>2</sub> by O<sub>3</sub>, contributed to the important formation of organic nitrate by initializing the production of nitrooxy  
316 peroxy radicals (Ng et al., 2008; Rollins et al., 2012). Laboratory studies (Nakayama et al., 2013; Liu et al., 2015c) also widely  
317 observed the rapid production of nitrogen-containing OA involving NO<sub>x</sub> chemistry could contribute to light absorption of  
318 aerosols.

319 Overall, by apportioning the absorption of primary and secondary BrC, we found the photochemical processes led to an  
320 enhanced contribution of fraction of absorbance of secondary BrC to total absorbance by 30% but reduced contribution of  
321 primary BrC about 20% in the semi-urban environment. Fig. 4b showed that the MAC of POA decreased after the morning  
322 peak. The MAC of SOA showed an afternoon peak (Fig. 4c), indicating the enhancement of absorption efficiency of secondary  
323 BrC, which occurred in a few hours after the peak solar radiation. This revealed that the whitening and darkening of BrC  
324 occurred simultaneously, and the secondary BrC produced by photooxidation may compensate some bleaching effect of  
325 primary BrC. The dominance of both competing processes may depend on the timescale and altitude in the atmosphere. For  
326 example, the enhanced BrC fraction observed above the planetary boundary layer may be explained by the enhanced secondary  
327 BrC (Tian et al., 2020), while further ageing may bleach the produced chromophores of these SOA.



328  
329  
330  
331  
332  
333

**Figure 4. Diurnal variations of absorption coefficient at  $\lambda=375\text{nm}$  ( $\sigma_{\text{abs},375}$ ) for BC (a), primary BrC and absorption efficiency of primary BrC ( $\sigma_{\text{abs,pri BrC}}/\text{POA}$ ) is shown in shade (b), secondary BrC and absorption efficiency of secondary BrC ( $\sigma_{\text{abs,sec BrC}}/\text{SOA}$ ) is shown in shade, along with the  $\text{C}_x\text{H}_y\text{N}_z$  and  $\text{C}_x\text{H}_y\text{N}_z\text{O}_p$  fragments (c); the respective fraction in total for the segregated  $\sigma_{\text{abs},375}$  (d-f), with direct radiation shown in shade. In each plot, the lines, dots and whiskers denote the median, mean and the 25th/75th percentiles at each hour respectively.**

334

#### 4. Conclusion

335

This study apportioned the shortwave absorption of BC, primary and secondary BrC, through concurrent measurements of BC microphysical properties and OA mass spectra. The apportioned primary BrC absorption was linked with traffic and biomass burning emissions, while secondary BrC was found to be associated with an oxygenated secondary OA factor with higher nitrogen content. The enhancement of secondary BrC and decrease of primary BrC simultaneously occurred via daytime photooxidation. The results emphasize the importance of nitrogen-containing OA in contributing to BrC. These OA could primarily emit as aerosol phase, or in gas phase which requires further oxidation to be in aerosol phase to serve as BrC. The  $\text{NO}_x$ -involved chemistry is prone to add nitrogen element to the existing OA and enhance the absorptivity of chromophores. The anthropogenic  $\text{NO}_x$  emission could be therefore an important source in producing shortwave absorbing components in the atmosphere, which may offset some of the conventionally-thought photobleaching of BrC by photochemistry. The production of secondary BrC should be considered when assessing the environment and climate impacts of light-absorbing aerosols.

344

345 **Acknowledgments**

346 This research was supported by the National Natural Science Foundation of China (Grant No. 42175116 and 41875167),  
347 National Key R&D Program of China (2019YFC0214703).

348 **Author contribution**

349 D.L., X.J. and Qian L. prepared and designed the observation. D.L., Qian L., X.J and P.T. initiated the field campaign and  
350 conducted the measurements. Qian L., D.L. P.T., Y.W., S.L. and K.H. contributed to the data analysis. Qian L., H.M., L.R.,  
351 B.K., D.D. and S.K. provided technical support and assistance. Qian L. and D.L. wrote the manuscript. All authors read and  
352 approved the final manuscript.

353

354 **References**

- 355 Aiken, A. C., Salcedo, D., Cubison, M. J., Huffman, J. A., DeCarlo, P. F., Ulbrich, I. M., Docherty, K. S., Sueper, D., Kimmel,  
356 J. R., Worsnop, D. R., Trimborn, A., Northway, M., Stone, E. A., Schauer, J. J., Volkamer, R. M., Fortner, E., de Foy, B., Wang,  
357 J., Laskin, A., Shutthanandan, V., Zheng, J., Zhang, R., Gaffney, J., Marley, N. A., Paredes-Miranda, G., Arnott, W. P., Molina,  
358 L. T., Sosa, G., and Jimenez, J. L.: Mexico City aerosol analysis during MILAGRO using high resolution aerosol mass  
359 spectrometry at the urban supersite (T0) - Part 1: Fine particle composition and organic source apportionment, *Atmos Chem*  
360 *Phys*, 9, 6633-6653, 10.5194/acp-9-6633-2009, 2009.
- 361 Andreae, M. O. and Crutzen, P. J.: Atmospheric aerosols: Biogeochemical sources and role in atmospheric chemistry, *Science*,  
362 276, 1052-1058, doi:10.1126/science.276.5315.1052, 1997.
- 363 Bahadur, R., Praveen, P. S., Xu, Y., and Ramanathan, V.: Solar absorption by elemental and brown carbon determined from  
364 spectral observations, *Proceedings of the National Academy of Sciences of the United States of America*, 109, 17366-17371,  
365 doi:10.1073/pnas.1205910109, 2012.
- 366 Bond, T. C.: Spectral dependence of visible light absorption by carbonaceous particles emitted from coal combustion,  
367 *Geophysical Research Letters*, 28, 4075-4078, doi:10.1029/2001gl013652, 2001.
- 368 Bond, T. C. and Bergstrom, R. W.: Light absorption by carbonaceous particles: An investigative review, *Aerosol Science and*  
369 *Technology*, 40, 27-67, doi:10.1080/02786820500421521, 2006.
- 370 Brown, S. G., Lee, T., Roberts, P. T., and Collett, J. L., Jr.: Wintertime Residential Biomass Burning in Las Vegas, Nevada;  
371 Marker Components and Apportionment Methods, *Atmosphere*, 7, 10.3390/atmos7040058, 2016.
- 372 Bruns, E. A., Perraud, V., Zelenyuk, A., Ezell, M. J., Johnson, S. N., Yu, Y., Imre, D., Finlayson-Pitts, B. J., and Alexander, M.  
373 L.: Comparison of FTIR and Particle Mass Spectrometry for the Measurement of Particulate Organic Nitrates, *Environmental*  
374 *Science & Technology*, 44, 1056-1061, doi:10.1021/es9029864, 2010.
- 375 Canagaratna, M. R., Jimenez, J. L., Kroll, J. H., Chen, Q., Kessler, S. H., Massoli, P., Hildebrandt Ruiz, L., Fortner, E., Williams,  
376 L. R., Wilson, K. R., Surratt, J. D., Donahue, N. M., Jayne, J. T., and Worsnop, D. R.: Elemental ratio measurements of organic  
377 compounds using aerosol mass spectrometry: characterization, improved calibration, and implications, *Atmospheric Chemistry*  
378 *and Physics*, 15, 253-272, doi:10.5194/acp-15-253-2015, 2015.
- 379 Canagaratna, M. R., Jayne, J. T., Jimenez, J. L., Allan, J. D., Alfarra, M. R., Zhang, Q., Onasch, T. B., Drewnick, F., Coe, H.,  
380 Middlebrook, A., Delia, A., Williams, L. R., Trimborn, A. M., Northway, M. J., DeCarlo, P. F., Kolb, C. E., Davidovits, P., and  
381 Worsnop, D. R.: Chemical and microphysical characterization of ambient aerosols with the aerodyne aerosol mass spectrometer,  
382 *Mass Spectrometry Reviews*, 26, 185-222, doi:10.1002/mas.20115, 2007.
- 383 Cheng, Y., Engling, G., He, K. B., Duan, F. K., Ma, Y. L., Du, Z. Y., Liu, J. M., Zheng, M., and Weber, R. J.: Biomass burning  
384 contribution to Beijing aerosol, *Atmospheric Chemistry and Physics*, 13, 7765-7781, doi:10.5194/acp-13-7765-2013, 2013.
- 385 Coury, C. and Dillner, A. M.: A method to quantify organic functional groups and inorganic compounds in ambient aerosols  
386 using attenuated total reflectance FTIR spectroscopy and multivariate chemometric techniques, *Atmospheric Environment*, 42,



387 5923-5932, doi:10.1016/j.atmosenv.2008.03.026, 2008.

388 Crilley, L. R., Bloss, W. J., Yin, J., Beddows, D. C. S., Harrison, R. M., Allan, J. D., Young, D. E., Flynn, M., Williams, P.,  
389 Zotter, P., Prevot, A. S. H., Heal, M. R., Barlow, J. F., Halios, C. H., Lee, J. D., Szidat, S., and Mohr, C.: Sources and  
390 contributions of wood smoke during winter in London: assessing local and regional influences, *Atmos Chem Phys*, 15, 3149-  
391 3171, 10.5194/acp-15-3149-2015, 2015.

392 Cubison, M. J., Ortega, A. M., Hayes, P. L., Farmer, D. K., Day, D., Lechner, M. J., Brune, W. H., Apel, E., Diskin, G. S.,  
393 Fisher, J. A., Fuelberg, H. E., Hecobian, A., Knapp, D. J., Mikoviny, T., Riemer, D., Sachse, G. W., Sessions, W., Weber, R. J.,  
394 Weinheimer, A. J., Wisthaler, A., and Jimenez, J. L.: Effects of aging on organic aerosol from open biomass burning smoke in  
395 aircraft and laboratory studies, *Atmos Chem Phys*, 11, 12049-12064, 10.5194/acp-11-12049-2011, 2011.

396 Dasari, S., Andersson, A., Bikkina, S., Holmstrand, H., Budhavant, K., Satheesh, S., Asmi, E., Kesti, J., Backman, J., Salam,  
397 A., Bisht, D. S., Tiwari, S., Hameed, Z., and Gustafsson, O.: Photochemical degradation affects the light absorption of water-  
398 soluble brown carbon in the South Asian outflow, *Science Advances*, 5, 10.1126/sciadv.aau8066, 2019.

399 DeCarlo, P. F., Ulbrich, I. M., Crouse, J., de Foy, B., Dunlea, E. J., Aiken, A. C., Knapp, D., Weinheimer, A. J., Campos, T.,  
400 Wennberg, P. O., and Jimenez, J. L.: Investigation of the sources and processing of organic aerosol over the Central Mexican  
401 Plateau from aircraft measurements during MILAGRO, *Atmospheric Chemistry and Physics*, 10, 5257-5280, doi:10.5194/acp-  
402 10-5257-2010, 2010.

403 DeWitt, H. L., Hellebust, S., Temime-Roussel, B., Ravier, S., Polo, L., Jacob, V., Buisson, C., Charron, A., Andre, M., Pasquier,  
404 A., Besombes, J. L., Jaffrezo, J. L., Wortham, H., and Marchand, N.: Near-highway aerosol and gas-phase measurements in a  
405 high-diesel environment, *Atmospheric Chemistry and Physics*, 15, 4373-4387, doi:10.5194/acp-15-4373-2015, 2015.

406 Ding, S., Liu, D., Zhao, D., Hu, K., Tian, P., Zhou, W., Huang, M., Yang, Y., Wang, F., Sheng, J., Liu, Q., Kong, S., Cui, P.,  
407 Huang, Y., He, H., Coe, H., and Ding, D.: Size-Related Physical Properties of Black Carbon in the Lower Atmosphere over  
408 Beijing and Europe, *Environmental Science & Technology*, 53, 11112-11121, 10.1021/acs.est.9b03722, 2019.

409 Draxier, R. R. and Hess, G. D.: An overview of the HYSPLIT\_4 modelling system for trajectories, dispersion and deposition,  
410 *Australian Meteorological Magazine*, 47, 295-308, 1998.

411 Drinovec, L., Mo?Nik, G., Zotter, P., Prév?t, A. S. H., Ruckstuhl, C., Coz, E., Rupakheti, M., Sciare, J., Müller, T., and  
412 Wiedensohler, A.: The "dual-spot" Aethalometer: an improved measurement of aerosol black carbon with real-time loading  
413 compensation, *Atmospheric Measurement Techniques*, 8, 1965-1979, 2015a.

414 Drinovec, L., Močnik, G., Zotter, P., Prévôt, A. S. H., Ruckstuhl, C., Coz, E., Rupakheti, M., Sciare, J., Müller, T., Wiedensohler,  
415 A., and Hansen, A. D. A.: The "dual-spot" Aethalometer: an improved measurement of aerosol black carbon with real-time  
416 loading compensation, *Atmos. Meas. Tech.*, 8, 1965-1979, 10.5194/amt-8-1965-2015, 2015b.

417 Duesing, S., Wehner, B., Mueller, T., Stoecker, A., and Wiedensohler, A.: The effect of rapid relative humidity changes on fast  
418 filter-based aerosol-particle light-absorption measurements: uncertainties and correction schemes, *Atmospheric Measurement*  
419 *Techniques*, 12, 5879-5895, 10.5194/amt-12-5879-2019, 2019.

420 Ehn, M., Thornton, J. A., Kleist, E., Sipila, M., Junninen, H., Pullinen, I., Springer, M., Rubach, F., Tillmann, R., Lee, B.,

421 Lopez-Hilfiker, F., Andres, S., Acir, I.-H., Rissanen, M., Jokinen, T., Schobesberger, S., Kangasluoma, J., Kontkanen, J.,  
422 Nieminen, T., Kurten, T., Nielsen, L. B., Jorgensen, S., Kjaergaard, H. G., Canagaratna, M., Dal Maso, M., Berndt, T., Petaja,  
423 T., Wahner, A., Kerminen, V.-M., Kulmala, M., Worsnop, D. R., Wildt, J., and Mentel, T. F.: A large source of low-volatility  
424 secondary organic aerosol, *Nature*, 506, 476-+, doi:10.1038/nature13032, 2014.

425 Elser, M., Huang, R.-J., Wolf, R., Slowik, J. G., Wang, Q., Canonaco, F., Li, G., Bozzetti, C., Daellenbach, K. R., Huang, Y.,  
426 Zhang, R., Li, Z., Cao, J., Baltensperger, U., El-Haddad, I., and Prevot, A. S. H.: New insights into PM<sub>2.5</sub> chemical  
427 composition and sources in two major cities in China during extreme haze events using aerosol mass spectrometry, *Atmos*  
428 *Chem Phys*, 16, 3207-3225, 10.5194/acp-16-3207-2016, 2016.

429 Finewax, Z., de Gouw, J. A., and Ziemann, P. J.: Identification and Quantification of 4-Nitrocatechol Formed from OH and  
430 NO<sub>3</sub> Radical-Initiated Reactions of Catechol in Air in the Presence of NO<sub>x</sub>: Implications for Secondary Organic Aerosol  
431 Formation from Biomass Burning, *Environmental Science & Technology*, 52, 1981-1989, doi:10.1021/acs.est.7b05864, 2018.

432 Forrister, H., Liu, J., Scheuer, E., Dibb, J., Ziemba, L., Thornhill, K. L., Anderson, B., Diskin, G., Perring, A. E., Schwarz, J.  
433 P., Campuzano-Jost, P., Day, D. A., Palm, B. B., Jimenez, J. L., Nenes, A., and Weber, R. J.: Evolution of brown carbon in  
434 wildfire plumes, *Geophysical Research Letters*, 42, 4623-4630, doi:10.1002/2015gl063897, 2015.

435 Gentner, D. R., Isaacman, G., Worton, D. R., Chan, A. W. H., Dallmann, T. R., Davis, L., Liu, S., Day, D. A., Russell, L. M.,  
436 Wilson, K. R., Weber, R., Guha, A., Harley, R. A., and Goldstein, A. H.: Elucidating secondary organic aerosol from diesel and  
437 gasoline vehicles through detailed characterization of organic carbon emissions, *Proceedings of the National Academy of*  
438 *Sciences of the United States of America*, 109, 18318-18323, doi:10.1073/pnas.1212272109, 2012.

439 Gentner, D. R., Jathar, S. H., Gordon, T. D., Bahreini, R., Day, D. A., El Haddad, I., Hayes, P. L., Pieber, S. M., Platt, S. M.,  
440 de Gouw, J., Goldstein, A. H., Harley, R. A., Jimenez, J. L., Prevot, A. S. H., and Robinson, A. L.: Review of Urban Secondary  
441 Organic Aerosol Formation from Gasoline and Diesel Motor Vehicle Emissions, *Environmental Science & Technology*, 51,  
442 1074-1093, doi:10.1021/acs.est.6b04509, 2017.

443 Gilardoni, S., Massoli, P., Paglione, M., Giulianelli, L., Carbone, C., Rinaldi, M., Decesari, S., Sandrini, S., Costabile, F.,  
444 Gobbi, G. P., Pietrogrande, M. C., Visentin, M., Scotto, F., Fuzzi, S., and Facchini, M. C.: Direct observation of aqueous  
445 secondary organic aerosol from biomass-burning emissions, *Proceedings of the National Academy of Sciences of the United*  
446 *States of America*, 113, 10013-10018, 10.1073/pnas.1602212113, 2016.

447 Hayes, P. L., Ortega, A. M., Cubison, M. J., Froyd, K. D., Zhao, Y., Cliff, S. S., Hu, W. W., Toohey, D. W., Flynn, J. H., Lefer,  
448 B. L., Grossberg, N., Alvarez, S., Rappenglueck, B., Taylor, J. W., Allan, J. D., Holloway, J. S., Gilman, J. B., Kuster, W. C.,  
449 De Gouw, J. A., Massoli, P., Zhang, X., Liu, J., Weber, R. J., Corrigan, A. L., Russell, L. M., Isaacman, G., Worton, D. R.,  
450 Kreisberg, N. M., Goldstein, A. H., Thalman, R., Waxman, E. M., Volkamer, R., Lin, Y. H., Surratt, J. D., Kleindienst, T. E.,  
451 Offenberg, J. H., Dusanter, S., Griffith, S., Stevens, P. S., Brioude, J., Angevine, W. M., and Jimenez, J. L.: Organic aerosol  
452 composition and sources in Pasadena, California, during the 2010 CalNex campaign, *Journal of Geophysical Research-*  
453 *Atmospheres*, 118, 9233-9257, 10.1002/jgrd.50530, 2013.

454 Hu, K., Liu, D., Tian, P., Wu, Y., Deng, Z., Wu, Y., Zhao, D., Li, R., Sheng, J., Huang, M., Ding, D., Li, W., Wang, Y., and Wu,

455 Y.: Measurements of the Diversity of Shape and Mixing State for Ambient Black Carbon Particles, *Geophysical Research*  
456 *Letters*, 48, doi:10.1029/2021gl094522, 2021.

457 Hu, W., Hu, M., Hu, W.-W., Zheng, J., Chen, C., Wu, Y., and Guo, S.: Seasonal variations in high time-resolved chemical  
458 compositions, sources, and evolution of atmospheric submicron aerosols in the megacity Beijing, *Atmos Chem Phys*, 17, 9979-  
459 10000, 10.5194/acp-17-9979-2017, 2017.

460 Huang, D. D., Zhu, S., An, J., Wang, Q., Qiao, L., Zhou, M., He, X., Ma, Y., Sun, Y., Huang, C., Yu, J. Z., and Zhang, Q.:  
461 Comparative Assessment of Cooking Emission Contributions to Urban Organic Aerosol Using Online Molecular Tracers and  
462 Aerosol Mass Spectrometry Measurements, *Environmental Science & Technology*, 55, 14526-14535, 10.1021/acs.est.1c03280,  
463 2021.

464 Huffman, J. A., Docherty, K. S., Aiken, A. C., Cubison, M. J., Ulbrich, I. M., DeCarlo, P. F., Sueper, D., Jayne, J. T., Worsnop,  
465 D. R., Ziemann, P. J., and Jimenez, J. L.: Chemically-resolved aerosol volatility measurements from two megacity field studies,  
466 *Atmospheric Chemistry and Physics*, 9, 7161-7182, doi:10.5194/acp-9-7161-2009, 2009.

467 Jacobson, M. Z.: Isolating nitrated and aromatic aerosols and nitrated aromatic gases as sources of ultraviolet light absorption,  
468 *Journal of Geophysical Research-Atmospheres*, 104, 3527-3542, doi:10.1029/1998jd100054, 1999.

469 Jayne, J. T., Leard, D. C., Zhang, X. F., Davidovits, P., Smith, K. A., Kolb, C. E., and Worsnop, D. R.: Development of an  
470 aerosol mass spectrometer for size and composition analysis of submicron particles, *Aerosol Science and Technology*, 33, 49-  
471 70, 10.1080/027868200410840, 2000.

472 Jiang, X., Liu, D., Li, Q., Tian, P., Wu, Y., Li, S., Hu, K., Ding, S., Bi, K., Li, R., Huang, M., Ding, D., Chen, Q., Kong, S., Li,  
473 W., Pang, Y., and He, D.: Connecting the Light Absorption of Atmospheric Organic Aerosols with Oxidation State and Polarity,  
474 *Environmental science & technology*, 10.1021/acs.est.2c02202, 2022.

475 Jimenez, J. L., Canagaratna, M. R., Donahue, N. M., Prevot, A. S. H., Zhang, Q., Kroll, J. H., DeCarlo, P. F., Allan, J. D., Coe,  
476 H., Ng, N. L., Aiken, A. C., Docherty, K. S., Ulbrich, I. M., Grieshop, A. P., Robinson, A. L., Duplissy, J., Smith, J. D., Wilson,  
477 K. R., Lanz, V. A., Hueglin, C., Sun, Y. L., Tian, J., Laaksonen, A., Raatikainen, T., Rautiainen, J., Vaattovaara, P., Ehn, M.,  
478 Kulmala, M., Tomlinson, J. M., Collins, D. R., Cubison, M. J., Dunlea, E. J., Huffman, J. A., Onasch, T. B., Alfarra, M. R.,  
479 Williams, P. I., Bower, K., Kondo, Y., Schneider, J., Drewnick, F., Borrmann, S., Weimer, S., Demerjian, K., Salcedo, D.,  
480 Cottrell, L., Griffin, R., Takami, A., Miyoshi, T., Hatakeyama, S., Shimono, A., Sun, J. Y., Zhang, Y. M., Dzepina, K., Kimmel,  
481 J. R., Sueper, D., Jayne, J. T., Herndon, S. C., Trimborn, A. M., Williams, L. R., Wood, E. C., Middlebrook, A. M., Kolb, C.  
482 E., Baltensperger, U., and Worsnop, D. R.: Evolution of Organic Aerosols in the Atmosphere, *Science*, 326, 1525-1529,  
483 doi:10.1126/science.1180353, 2009.

484 Keyte, I. J., Albinet, A., and Harrison, R. M.: On-road traffic emissions of polycyclic aromatic hydrocarbons and their oxy-  
485 and nitro-derivative compounds measured in road tunnel environments, *Science of the Total Environment*, 566, 1131-1142,  
486 doi:10.1016/j.scitotenv.2016.05.152, 2016.

487 Laborde, M., Schnaiter, M., Linke, C., Saathoff, H., Naumann, K. H., Moehler, O., Berlenz, S., Wagner, U., Taylor, J. W., Liu,  
488 D., Flynn, M., Allan, J. D., Coe, H., Heimerl, K., Dahlkoetter, F., Weinzierl, B., Wollny, A. G., Zanutta, M., Cozic, J., Laj, P.,

489 Hitzenberger, R., Schwarz, J. P., and Gysel, M.: Single Particle Soot Photometer intercomparison at the AIDA chamber,  
490 Atmospheric Measurement Techniques, 5, 3077-3097, doi:10.5194/amt-5-3077-2012, 2012.

491 Laskin, A., Laskin, J., and Nizkorodov, S. A.: Chemistry of Atmospheric Brown Carbon, Chemical Reviews, 115, 4335-4382,  
492 doi:10.1021/cr5006167, 2015.

493 Liebmann, J., Sobanski, N., Schuladen, J., Karu, E., Hellen, H., Hakola, H., Zha, Q., Ehn, M., Riva, M., Heikkinen, L.,  
494 Williams, J., Fischer, H., Lelieyeld, J., and Crowley, J. N.: Alkyl nitrates in the boreal forest: formation via the NO<sub>3</sub>-, OH- and  
495 O<sub>3</sub>-induced oxidation of biogenic volatile organic compounds and ambient lifetimes, Atmospheric Chemistry and Physics,  
496 19, 10391-10403, doi:10.5194/acp-19-10391-2019, 2019.

497 Lin, P., Liu, J., Shilling, J. E., Kathmann, S. M., Laskin, J., and Laskin, A.: Molecular characterization of brown carbon (BrC)  
498 chromophores in secondary organic aerosol generated from photo-oxidation of toluene, Physical Chemistry Chemical Physics,  
499 17, 23312-23325, doi:10.1039/c5cp02563j, 2015.

500 Liu, D., He, C., Schwarz, J. P., and Wang, X.: Lifecycle of light-absorbing carbonaceous aerosols in the atmosphere, npj  
501 Climate and Atmospheric Science, 3, 40, doi:10.1038/s41612-020-00145-8, 2020.

502 Liu, D., Taylor, J. W., Young, D. E., Flynn, M. J., Coe, H., and Allan, J. D.: The effect of complex black carbon microphysics  
503 on the determination of the optical properties of brown carbon, Geophysical Research Letters, 42, 613-619,  
504 doi:10.1002/2014gl062443, 2015a.

505 Liu, D., Allan, J. D., Young, D. E., Coe, H., Beddows, D., Fleming, Z. L., Flynn, M. J., Gallagher, M. W., Harrison, R. M., Lee,  
506 J., Prevot, A. S. H., Taylor, J. W., Yin, J., Williams, P. I., and Zotter, P.: Size distribution, mixing state and source apportionment  
507 of black carbon aerosol in London during wintertime, Atmos Chem Phys, 14, 10061-10084, 10.5194/acp-14-10061-2014, 2014.

508 Liu, D., Joshi, R., Wang, J., Yu, C., Allan, J. D., Coe, H., Flynn, M. J., Xie, C., Lee, J., Squires, F., Kotthaus, S., Grimmond,  
509 S., Ge, X., Sun, Y., and Fu, P.: Contrasting physical properties of black carbon in urban Beijing between winter and summer,  
510 Atmospheric Chemistry and Physics, 19, 6749-6769, doi:10.5194/acp-19-6749-2019, 2019a.

511 Liu, D., Joshi, R., Wang, J., Yu, C., Allan, J. D., Coe, H., Flynn, M. J., Xie, C., Lee, J., Squires, F., Kotthaus, S., Grimmond,  
512 S., Ge, X., Sun, Y., and Fu, P.: Contrasting physical properties of black carbon in urban Beijing between winter and summer,  
513 Atmos. Chem. Phys., 19, 6749-6769, doi:10.5194/acp-19-6749-2019, 2019b.

514 Liu, D., Li, S., Hu, D., Kong, S., Cheng, Y., Wu, Y., Ding, S., Hu, K., Zheng, S., Yan, Q., Zheng, H., Zhao, D., Tian, P., Ye, J.,  
515 Huang, M., and Ding, D.: Evolution of Aerosol Optical Properties from Wood Smoke in Real Atmosphere Influenced by  
516 Burning Phase and Solar Radiation, Environmental Science & Technology, 55, 5677-5688, 10.1021/acs.est.0c07569, 2021.

517 Liu, F., Zhang, Q., Tong, D., Zheng, B., Li, M., Huo, H., and He, K. B.: High-resolution inventory of technologies, activities,  
518 and emissions of coal-fired power plants in China from 1990 to 2010, Atmospheric Chemistry and Physics, 15, 13299-13317,  
519 doi:10.5194/acp-15-13299-2015, 2015b.

520 Liu, J., Mauzerall, D. L., Chen, Q., Zhang, Q., Song, Y., Peng, W., Klimont, Z., Qiu, X., Zhang, S., Hu, M., Lin, W., Smith, K.  
521 R., and Zhu, T.: Air pollutant emissions from Chinese households: A major and underappreciated ambient pollution source,  
522 Proceedings of the National Academy of Sciences of the United States of America, 113, 7756-7761,

523 doi:10.1073/pnas.1604537113, 2016.

524 Liu, P. F., Abdelmalki, N., Hung, H. M., Wang, Y., Brune, W. H., and Martin, S. T.: Ultraviolet and visible complex refractive  
525 indices of secondary organic material produced by photooxidation of the aromatic compounds toluene and m-xylene,  
526 Atmospheric Chemistry and Physics, 15, 1435-1446, doi:10.5194/acp-15-1435-2015, 2015c.

527 Makra, L., Matyasovszky, I., Guba, Z., Karatzas, K., and Anttila, P.: Monitoring the long-range transport effects on urban  
528 PM10 levels using 3D clusters of backward trajectories, Atmospheric Environment, 45, 2630-2641,  
529 doi:10.1016/j.atmosenv.2011.02.068, 2011.

530 Middlebrook, A. M., Bahreini, R., Jimenez, J. L., and Canagaratna, M. R.: Evaluation of Composition-Dependent Collection  
531 Efficiencies for the Aerodyne Aerosol Mass Spectrometer using Field Data, Aerosol Science and Technology, 46, 258-271,  
532 10.1080/02786826.2011.620041, 2012.

533 Mohr, C., DeCarlo, P. F., Heringa, M. F., Chirico, R., Slowik, J. G., Richter, R., Reche, C., Alastuey, A., Querol, X., Seco, R.,  
534 Penuelas, J., Jimenez, J. L., Crippa, M., Zimmermann, R., Baltensperger, U., and Prevot, A. S. H.: Identification and  
535 quantification of organic aerosol from cooking and other sources in Barcelona using aerosol mass spectrometer data,  
536 Atmospheric Chemistry and Physics, 12, 1649-1665, doi:10.5194/acp-12-1649-2012, 2012.

537 Nakayama, T., Sato, K., Matsumi, Y., Imamura, T., Yamazaki, A., and Uchiyama, A.: Wavelength and NO<sub>x</sub> dependent complex  
538 refractive index of SOAs generated from the photooxidation of toluene, Atmospheric Chemistry and Physics, 13, 531-545,  
539 doi:10.5194/acp-13-531-2013, 2013.

540 Ng, N. L., Kwan, A. J., Surratt, J. D., Chan, A. W. H., Chhabra, P. S., Sorooshian, A., Pye, H. O. T., Crounse, J. D., Wennberg,  
541 P. O., Flagan, R. C., and Seinfeld, J. H.: Secondary organic aerosol (SOA) formation from reaction of isoprene with nitrate  
542 radicals (NO<sub>3</sub>), Atmospheric Chemistry and Physics, 8, 4117-4140, doi:10.5194/acp-8-4117-2008, 2008.

543 Paatero, P. and Tapper, U.: POSITIVE MATRIX FACTORIZATION - A NONNEGATIVE FACTOR MODEL WITH  
544 OPTIMAL UTILIZATION OF ERROR-ESTIMATES OF DATA VALUES, Environmetrics, 5, 111-126,  
545 doi:10.1002/env.3170050203, 1994.

546 Pachon, J. E., Weber, R. J., Zhang, X., Mulholland, J. A., and Russell, A. G.: Revising the use of potassium (K) in the source  
547 apportionment of PM<sub>2.5</sub>, Atmospheric Pollution Research, 4, 14-21, 10.5094/apr.2013.002, 2013.

548 Palm, B. B., Peng, Q., Fredrickson, C. D., Lee, B. H., Garofalo, L. A., Pothier, M. A., Kreidenweis, S. M., Farmer, D. K.,  
549 Pokhrel, R. P., Shen, Y., Murphy, S. M., Permar, W., Hu, L., Campos, T. L., Hall, S. R., Ullmann, K., Zhang, X., Flocke, F.,  
550 Fischer, E. V., and Thornton, J. A.: Quantification of organic aerosol and brown carbon evolution in fresh wildfire plumes,  
551 Proceedings of the National Academy of Sciences of the United States of America, 117, 29469-29477,  
552 10.1073/pnas.2012218117, 2020.

553 Rizzo, L. V., Artaxo, P., Mueller, T., Wiedensohler, A., Paixao, M., Cirino, G. G., Arana, A., Swietlicki, E., Roldin, P., Fors, E.  
554 O., Wiedemann, K. T., Leal, L. S. M., and Kulmala, M.: Long term measurements of aerosol optical properties at a primary  
555 forest site in Amazonia, Atmospheric Chemistry and Physics, 13, 2391-2413, doi:10.5194/acp-13-2391-2013, 2013.

556 Rollins, A. W., Browne, E. C., Min, K. E., Pusede, S. E., Wooldridge, P. J., Gentner, D. R., Goldstein, A. H., Liu, S., Day, D.

557 A., Russell, L. M., and Cohen, R. C.: Evidence for NO<sub>x</sub> Control over Nighttime SOA Formation, *Science*, 337, 1210-1212,  
558 doi:10.1126/science.1221520, 2012.

559 Satish, R. and Rastogi, N.: On the Use of Brown Carbon Spectra as a Tool to Understand Their Broader Composition and  
560 Characteristics: A Case Study from Crop-residue Burning Samples, *Acs Omega*, 4, 1847-1853, 10.1021/acsomega.8b02637,  
561 2019.

562 Satish, R., Shamjad, P., Thamban, N., Tripathi, S., and Rastogi, N.: Temporal Characteristics of Brown Carbon over the Central  
563 Indo-Gangetic Plain, *Environmental Science & Technology*, 51, 6765-6772, 10.1021/acs.est.7b00734, 2017.

564 Schnitzler, E. G., Liu, T., Hems, R. F., and Abbatt, J. P. D.: Emerging investigator series: heterogeneous OH oxidation of  
565 primary brown carbon aerosol: effects of relative humidity and volatility, *Environmental Science-Processes & Impacts*, 22,  
566 2162-2171, 10.1039/d0em00311e, 2020.

567 Schuetzle, D.: SAMPLING OF VEHICLE EMISSIONS FOR CHEMICAL-ANALYSIS AND BIOLOGICAL TESTING,  
568 *Environmental Health Perspectives*, 47, 65-80, doi:10.2307/3429500, 1983.

569 Schwarz, J. P., Spackman, J. R., Fahey, D. W., Gao, R. S., Lohmann, U., Stier, P., Watts, L. A., Thomson, D. S., Lack, D. A.,  
570 Pfister, L., Mahoney, M. J., Baumgardner, D., Wilson, J. C., and Reeves, J. M.: Coatings and their enhancement of black carbon  
571 light absorption in the tropical atmosphere, *Journal of Geophysical Research-Atmospheres*, 113, 10.1029/2007jd009042, 2008.

572 Shen, G., Ru, M., Du, W., Zhu, X., Zhong, Q., Chen, Y., Shen, H., Yun, X., Meng, W., Liu, J., Cheng, H., Hu, J., Guan, D., and  
573 Tao, S.: Impacts of air pollutants from rural Chinese households under the rapid residential energy transition, *Nature*  
574 *Communications*, 10, doi:10.1038/s41467-019-11453-w, 2019.

575 Siemens, K., Morales, A., He, Q., Li, C., Hettiyadura, A. P. S., Rudich, Y., and Laskin, A.: Molecular Analysis of Secondary  
576 Brown Carbon Produced from the Photooxidation of Naphthalene, *Environmental science & technology*, 56, 3340-3353,  
577 doi:10.1021/acs.est.1c03135, 2022.

578 Sun, Y., Jiang, Q., Wang, Z., Fu, P., Li, J., Yang, T., and Yin, Y.: Investigation of the sources and evolution processes of severe  
579 haze pollution in Beijing in January 2013, *Journal of Geophysical Research-Atmospheres*, 119, 4380-4398,  
580 doi:10.1002/2014jd021641, 2014.

581 Sun, Y., Du, W., Fu, P., Wang, Q., Li, J., Ge, X., Zhang, Q., Zhu, C., Ren, L., Xu, W., Zhao, J., Han, T., Worsnop, D. R., and  
582 Wang, Z.: Primary and secondary aerosols in Beijing in winter: sources, variations and processes, *Atmos Chem Phys*, 16, 8309-  
583 8329, 10.5194/acp-16-8309-2016, 2016.

584 Sun, Y. L., Zhang, Q., Schwab, J. J., Chen, W. N., Bae, M. S., Lin, Y. C., Hung, H. M., and Demerjian, K. L.: A case study of  
585 aerosol processing and evolution in summer in New York City, *Atmos Chem Phys*, 11, 12737-12750, 10.5194/acp-11-12737-  
586 2011, 2011a.

587 Sun, Y. L., Zhang, Q., Schwab, J. J., Demerjian, K. L., Chen, W. N., Bae, M. S., Hung, H. M., Hogrefe, O., Frank, B., Rattigan,  
588 O. V., and Lin, Y. C.: Characterization of the sources and processes of organic and inorganic aerosols in New York city with a  
589 high-resolution time-of-flight aerosol mass spectrometer, *Atmospheric Chemistry and Physics*, 11, 1581-1602,  
590 doi:10.5194/acp-11-1581-2011, 2011b.

591 Taylor, J. W., Allan, J. D., Liu, D., Flynn, M., Weber, R., Zhang, X., Lefer, B. L., Grossberg, N., Flynn, J., and Coe, H.:  
592 Assessment of the sensitivity of core/shell parameters derived using the single-particle soot photometer to density and  
593 refractive index, *Atmospheric Measurement Techniques*, 8, 1701-1718, doi:10.5194/amt-8-1701-2015, 2015.

594 Tian, P., Liu, D., Zhao, D., Yu, C., Liu, Q., Huang, M., Deng, Z., Ran, L., Wu, Y., Ding, S., Hu, K., Zhao, G., Zhao, C., and  
595 Ding, D.: In situ vertical characteristics of optical properties and heating rates of aerosol over Beijing, *Atmospheric Chemistry  
596 and Physics*, 20, 2603-2622, doi:10.5194/acp-20-2603-2020, 2020.

597 Ulbrich, I. M., Canagaratna, M. R., Zhang, Q., Worsnop, D. R., and Jimenez, J. L.: Interpretation of organic components from  
598 Positive Matrix Factorization of aerosol mass spectrometric data, *Atmos Chem Phys*, 9, 2891-2918, 10.5194/acp-9-2891-2009,  
599 2009.

600 Updyke, K. M., Nguyen, T. B., and Nizkorodov, S. A.: Formation of brown carbon via reactions of ammonia with secondary  
601 organic aerosols from biogenic and anthropogenic precursors, *Atmospheric Environment*, 63, 22-31,  
602 doi:10.1016/j.atmosenv.2012.09.012, 2012.

603 Wang, Q., Han, Y., Ye, J., Liu, S., Pongpiachan, S., Zhang, N., Han, Y., Tian, J., Wu, C., Long, X., Zhang, Q., Zhang, W., Zhao,  
604 Z., and Cao, J.: High Contribution of Secondary Brown Carbon to Aerosol Light Absorption in the Southeastern Margin of  
605 Tibetan Plateau, *Geophysical Research Letters*, 46, 4962-4970, 10.1029/2019gl082731, 2019a.

606 Wang, Q., Cao, J., Han, Y., Tian, J., Zhang, Y., Pongpiachan, S., Zhang, Y., Li, L., Niu, X., Shen, Z., Zhao, Z., Tipmanee, D.,  
607 Bunsomboonsakul, S., Chen, Y., and Sun, J.: Enhanced light absorption due to the mixing state of black carbon in fresh biomass  
608 burning emissions, *Atmospheric Environment*, 180, 184-191, doi:10.1016/j.atmosenv.2018.02.049, 2018a.

609 Wang, X., Heald, C. L., Liu, J., Weber, R. J., Campuzano-Jost, P., Jimenez, J. L., Schwarz, J. P., and Perring, A. E.: Exploring  
610 the observational constraints on the simulation of brown carbon, *Atmos Chem Phys*, 18, 635-653, 10.5194/acp-18-635-2018,  
611 2018b.

612 Wang, X., Heald, C. L., Ridley, D. A., Schwarz, J. P., Spackman, J. R., Perring, A. E., Coe, H., Liu, D., and Clarke, A. D.:  
613 Exploiting simultaneous observational constraints on mass and absorption to estimate the global direct radiative forcing of  
614 black carbon and brown carbon, *Atmospheric Chemistry and Physics*, 14, 10989-11010, doi:10.5194/acp-14-10989-2014, 2014.

615 Wang, Y., Hu, M., Wang, Y., Zheng, J., Shang, D., Yang, Y., Liu, Y., Li, X., Tang, R., Zhu, W., Du, Z., Wu, Y., Guo, S., Wu, Z.,  
616 Lou, S., Hallquist, M., and Yu, J. Z.: The formation of nitro-aromatic compounds under high NO<sub>x</sub> and anthropogenic VOC  
617 conditions in urban Beijing, China, *Atmospheric Chemistry and Physics*, 19, 7649-7665, doi:10.5194/acp-19-7649-2019,  
618 2019b.

619 Wu, C. and Yu, J. Z.: Determination of primary combustion source organic carbon-to-elemental carbon (OC<sub>Euro</sub>-/aEuro-EC)  
620 ratio using ambient OC and EC measurements: secondary OC-EC correlation minimization method, *Atmos Chem Phys*, 16,  
621 5453-5465, 10.5194/acp-16-5453-2016, 2016.

622 Yang, W., Zhang, Y., Wang, X., Li, S., Zhu, M., Yu, Q., Li, G., Huang, Z., Zhang, H., Wu, Z., Song, W., Tan, J., and Shao, M.:  
623 Volatile organic compounds at a rural site in Beijing: influence of temporary emission control and wintertime heating,  
624 *Atmospheric Chemistry and Physics*, 18, 12663-12682, doi:10.5194/acp-18-12663-2018, 2018.

625 Yao, Z., Shen, X., Ye, Y., Cao, X., Jiang, X., Zhang, Y., and He, K.: On-road emission characteristics of VOCs from diesel  
626 trucks in Beijing, China, *Atmospheric Environment*, 103, 87-93, doi:10.1016/j.atmosenv.2014.12.028, 2015.

627 Zhang, Q., Worsnop, D. R., Canagaratna, M. R., and Jimenez, J. L.: Hydrocarbon-like and oxygenated organic aerosols in  
628 Pittsburgh: insights into sources and processes of organic aerosols, *Atmos Chem Phys*, 5, 3289-3311, 10.5194/acp-5-3289-  
629 2005, 2005.

630 Zhang, Q., Jimenez, J. L., Canagaratna, M. R., Ulbrich, I. M., Ng, N. L., Worsnop, D. R., and Sun, Y.: Understanding  
631 atmospheric organic aerosols via factor analysis of aerosol mass spectrometry: a review, *Analytical and Bioanalytical*  
632 *Chemistry*, 401, 3045-3067, doi:10.1007/s00216-011-5355-y, 2011.

633 Zhang, Q., Shen, Z., Zhang, L., Zeng, Y., Ning, Z., Zhang, T., Lei, Y., Wang, Q., Li, G., Sun, J., Westerdahl, D., Xu, H., and  
634 Cao, J.: Investigation of Primary and Secondary Particulate Brown Carbon in Two Chinese Cities of Xi'an and Hong Kong in  
635 Wintertime, *Environmental Science & Technology*, 54, 3803-3813, 10.1021/acs.est.9b05332, 2020.

636 Zhang, Y., Zhang, Q., Cheng, Y., Su, H., Li, H., Li, M., Zhang, X., Ding, A., and He, K.: Amplification of light absorption of  
637 black carbon associated with air pollution, *Atmospheric Chemistry and Physics*, 18, 9879-9896, doi:10.5194/acp-18-9879-  
638 2018, 2018.

639 Zhao, R., Lee, A. K. Y., Huang, L., Li, X., Yang, F., and Abbatt, J. P. D.: Photochemical processing of aqueous atmospheric  
640 brown carbon, *Atmospheric Chemistry and Physics*, 15, 6087-6100, doi:10.5194/acp-15-6087-2015, 2015.

641 Zhou, S., Collier, S., Xu, J., Mei, F., Wang, J., Lee, Y.-N., Sedlacek, A. J., III, Springston, S. R., Sun, Y., and Zhang, Q.:  
642 Influences of upwind emission sources and atmospheric processing on aerosol chemistry and properties at a rural location in  
643 the Northeastern US, *Journal of Geophysical Research-Atmospheres*, 121, 6049-6065, 10.1002/2015jd024568, 2016.

644  
645